Electronic Supplementing Information (ESI)

Understading the structural and charge transport property relationships for a variety of merocyanine single-crystals: a bottom up computational investigation.

Nora Gildemeister[a], Gaetano Ricci[b], Lukas Böhner[a], Jörg M. Neudörfl[f], Dirk Hertel[a], Frank Würthner[d,e], Fabrizia Negri[b,e*], Klaus Meerholz[a*], Daniele Fazzi[a*]

[a]Institut für Physikalische Chemie, Department für Chemie, Universität zu Köln, Greinstr. 4-6, 50939, Köln, Germany
D-50939 Köln, Germany.
[b]Università di Bologna, Dipartimento di Chimica 'Giacomo Ciamician', Via F. Selmi, 2, 40126 Bologna, Italy.
[c] Institut für Organische Chemie, Universität Würzburg, Am Hubland, 97074 Würzburg, Germany
[d] Center for Nanosystems Chemistry, Universität Würzburg, Am Hubland, 97074 Würzburg, Germany
[e]INSTM UdR Bologna, Via F. Selmi, 2, 40126 Bologna, Italy.
[f]Institut für Organische Chemie, Department für Chemie, Universität zu Köln, Greinstr. 4-6, 50939, Köln, Germany

E-mail: fabrizia.negri@unibo.it; klaus.meerholz@uni-koeln.de; dfazzi@uni-koeln.de

Table of Contents

1. Bond Length Alternation Pattern Analysis

D1A1

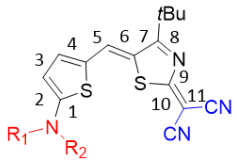

pyrl: R_1=R_2=-$[CH_2]_4$-
et/bu:R_1=Et R_2=*n*Bu
nbu: R_1=R_2=*n*Bu
nhex: R_1=R_2=*n*hex

D1A2

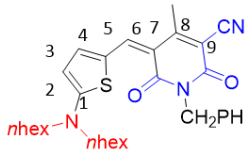

D1A3

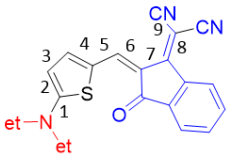

D2A1

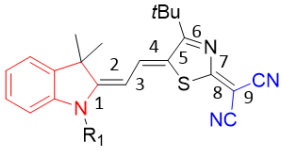

nbu: R_1=*n*Bu
nhex: R_1=*n*hex

D2A2

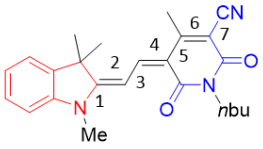

D2A3

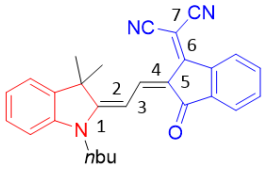

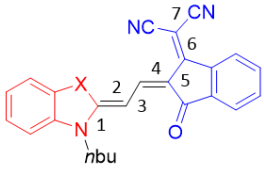

nbu(O): X=O
nbu(S): X=S

Figure S1: Molecular structures of merocyanines investigated in the study. Red and blue domains indicate the region where positive and negative partial charges were constrained during the C-DFT calculations (see main text).

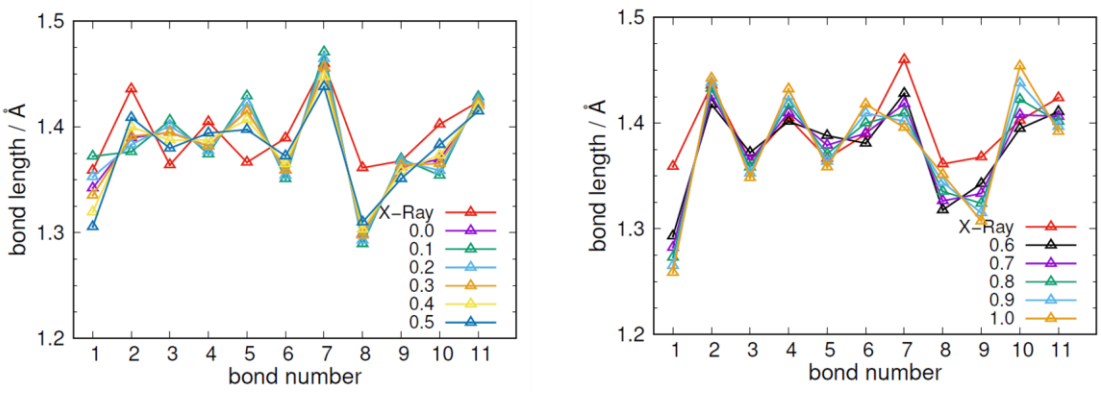

Figure S2: Computed BLA patterns (as defined by bond numbering in Figure **S1**) for different values of the partial charges (|δ| = 0.0q - 1.0q, q is the electronic charge) as constrained on *pyrl*-**D1A1** (C-DFT calculations, CAM-B3LYP-D3/6-311G*). Red line represents the BLA pattern as derived from the crystal structure.

Table S1: d_{BLA} values (see main text) of the neutral ground state, as defined by the difference between the average of single and double bonds (d_{BLA}^{average}) and as defined by the difference between the central bonds (d_{BLA}^{central}), for different values of the constrained partial charges (C-DFT: CAM-B3LYP-D3/6-311G*).

Molecule	$\delta^{D/A}$	d_{BLA}^{average} Å	d_{BLA}^{central} Å
pyrl-**D1A1**	±0.0q	0.039	0.056
	±0.1q	0.064	0.078
	±0.2q	0.052	0.069
	±0.3q	0.039	0.056
	±0.4q	0.024	0.042
	±0.5q	0.007	0.025
	±0.6q	-0.010	0.007
	±0.7q	-0.028	-0.011
	±0.8q	-0.046	-0.029
	±0.9q	-0.062	-0.046
	±1.0q	-0.076	-0.060
nbu-**D1A2**	±0.4q	0.004	0.012
	±0.5q	-0.011	-0.005
	±0.6q	-0.025	-0.022
	±0.7q	-0.039	-0.039
et-**D1A3**	±0.4q	0.006	0.016

	±0.5q	-0.011	-0.005
	±0.6q	-0.028	-0.026
	±0.7q	-0.043	-0.046
nhex-**D2A1**	±0.5q	0.019	0.010
	±0.6q	0.003	-0.007
	±0.7q	-0.014	-0.024
me/nbu-**D2A2**	±0.0q	0.040	0.032
	±0.1q	0.057	0.054
	±0.2q	0.048	0.041
	±0.3q	0.038	0.027
	±0.4q	0.027	0.012
	±0.5q	0.015	-0.003
	±0.6q	0.004	-0.018
	±0.7q	-0.008	-0.033
	±0.8q	-0.020	-0.048
	±0.9q	-0.030	-0.062
	±1.0q	-0.040	-0.074
nbu-**D2A3**	±0.4q	0.023	0.007
	±0.5q	0.008	-0.013
	±0.6q	-0.008	-0.034
	±0.7q	-0.024	-0.054
	±0.8q	-0.038	-0.072

To note that differences amongst strategies (*i-iii*) (see main text) in the prediction of the BLAs in the charged state are negligible (see Table S2 and S4). Regardless the method and approach adopted, the computed d_{BLA} in the cationic state are always negative, reflecting a zwitterionic- or cyanine-like character of the charged state. Such feature is almost independent by the choice of the $\delta^{D/A}$ in C-DFT, or the solvent in DFT/PCM. For such reason, we primarily referred the numerical variations of λ_i^h to the displacement of the neutral ground state PES rather than that occurring on the charged state.

Table S2: d_{BLA} values of the neutral and charged ground states, as defined by the difference between the average of single and double bonds (d_{BLA}^{average}) and as defined by the difference between the central bonds (d_{BLA}^{central}), for different values of the constrained partial charges (C-DFT: CAM-B3LYP-D3/6-311G*).

Molecule	$\delta^{D/A}$	d_{BLA}^{average} neutral GS Å	d_{BLA}^{average} charged GS Å	d_{BLA}^{central} neutral GS Å	d_{BLA}^{central} charged GS Å
pyrl-**D1A1**	±0.0q	0.039	-0.018	0.056	-0.026
	±0.1q	0.064	-0.010	0.078	-0.026
	±0.2q	0.052	-0.018	0.069	-0.026
	±0.3q	0.039	-0.018	0.056	-0.026
	±0.4q	0.024	-0.018	0.042	-0.026
	±0.5q	0.007	-0.017	0.025	-0.025
	±0.6q	-0.010	-0.018	0.007	-0.026
	±0.7q	-0.028	-0.018	-0.011	-0.026
	±0.8q	-0.046	-0.018	-0.029	-0.026
	±0.9q	-0.062	-0.018	-0.046	-0.026
	±1.0q	-0.076	-0.018	-0.060	-0.015
me/nbu-**D2A2**	±0.0q	0.040	-0.013	0.032	-0.037
	±0.1q	0.057	-0.013	0.054	-0.037
	±0.2q	0.048	-0.013	0.041	-0.037
	±0.3q	0.038	-0.013	0.027	-0.037
	±0.4q	0.027	-0.013	0.012	-0.037
	±0.5q	0.015	-0.013	-0.003	-0.037
	±0.6q	0.004	-0.014	-0.018	-0.038
	±0.7q	-0.008	-0.014	-0.033	-0.039
	±0.8q	-0.020	-0.015	-0.048	-0.039

	±0.9q	-0.030	-0.015	-0.062	-0.040
	±1.0q	-0.040	-0.014	-0.074	-0.040

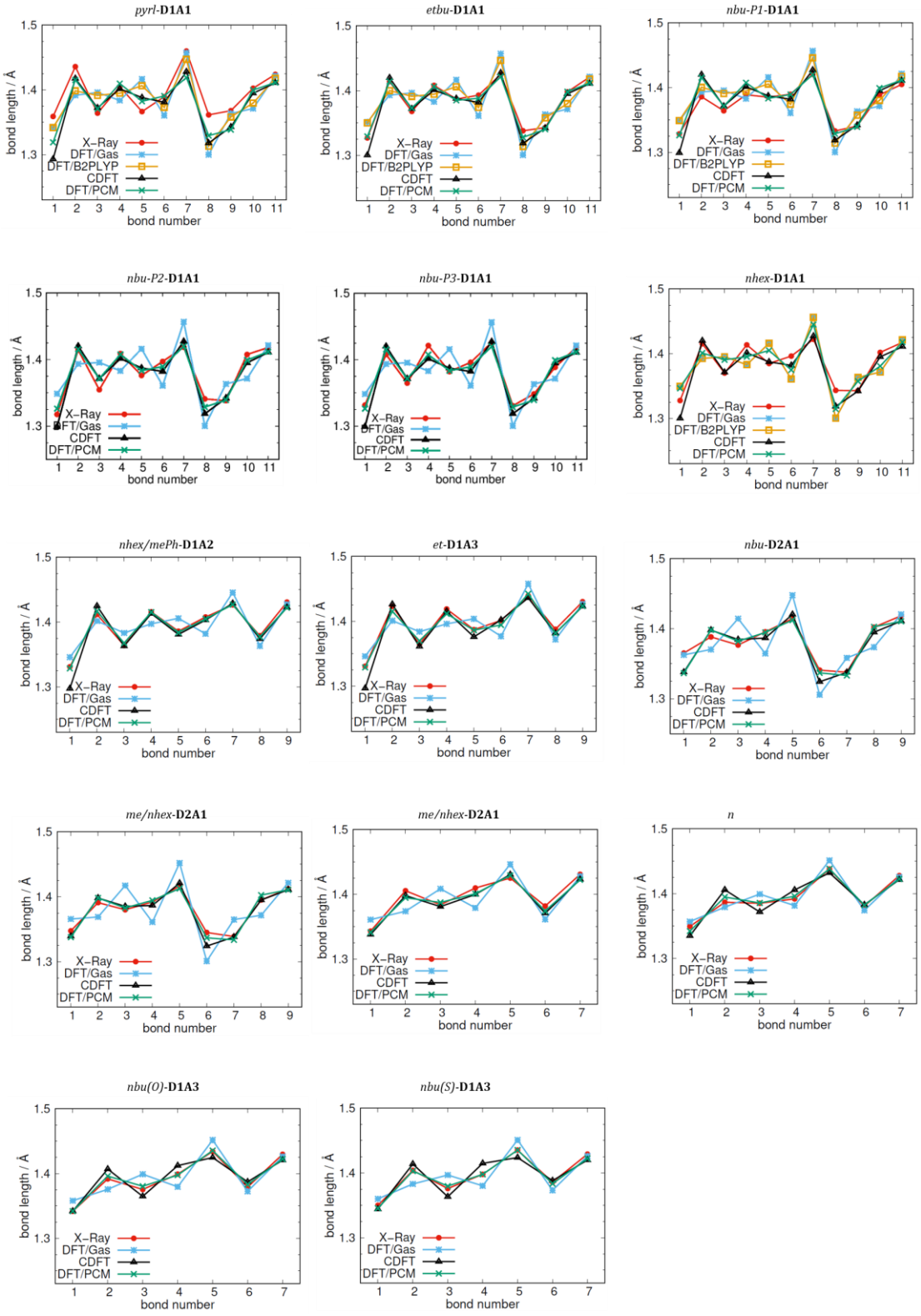

Figure S3: BLA patterns (as defined by bond numbering in **S1**) for all investigated merocyanines. Bond lengths (Å) from X-Ray single crystal data (red lines), DFT (ωB97X-D3/6-311G**, gas phase, blue lines), C-DFT (CAM-B3LYP-D3/6-311G**, $\delta^{D/A}$=±0.6q, gas phase, black lines), DFT (ωB97X-D/6-311G**, PCM (DMSO), green lines) and DFT (B2PLYP/def2-TZVP, gas phase, orange lines).

Table S3: d_{BLA} values of the neutral ground state as derived from X-Ray single crystal data, DFT (ωB97X-D3/6-311G**, gas), C-DFT (CAM-B3LYP-D3/6-311G**, $\delta^{D/A}$ = ±0.6q) and DFT/PCM (ωB97X-D3/6-311G**, a = chloroform, b = THF, c = acetone, d = DMSO).

		d_{BLA} average Å				d_{BLA} central Å			
class	side chain	X-Ray	DFT gas	C-DFT gas	DFT solvent	X-Ray	DFT gas	C-DFT gas	DFT solvent
D1A1	*pyrl*	-0.009	0.038 0.022[e]	-0.010	0.007[a] 0.000[b] -0.011[c] -0.015[d]	-0.023	0.056 0.033[e]	0.007	0.020[a] 0.011[b] -0.003[c] -0.008[d]
	et/bu	-0.012	0.039 0.022[e]	-0.010	0.007[a] 0.000[b] -0.011[c] -0.013[d]	-0.011	0.055 0.032[e]	0.005	0.020[a] 0.011[b] -0.003[c] -0.006[d]
	nbu-P1	-0.003	0.038 0.022[e]	-0.010	0.009[a] 0.002[b] -0.009[c] -0.013[d]	-0.004	0.056 0.031[e]	0.007	0.021[a] 0.012[b] -0.001[c] -0.006[d]
	nbu-P2	-0.010				-0.014			
	nbu-P3	-0.023				-0.021			
	nhex	-0.017	0.039 0.020[e]	-0.010	0.009[a] 0.002[b] -0.009[c] -0.013[d]	-0.011	0.055 0.030[e]	0.005	0.021[a] 0.012[b] -0.001[c] -0.006[d]
D1A2	*nhex/mePh*	-0.016	0.016	-0.025	-0.006[a] -0.010[b] -0.016[c] -0.018[d]	-0.022	0.024	-0.022	-0.005[a] -0.011[b] -0.018[c] -0.021[d]
D1A3	*et*	-0.017	0.017	-0.028	-0.002[a] -0.005[b] -0.009[c] -0.011[d]	-0.014	0.027	-0.026	0.003[a] -0.001[b] -0.006[c] -0.008[d]
D2A1	*nhex*	-0.002	0.054	0.003	0.013[a] 0.006[b] -0.004[c] -0.007[d]	-0.011	0.052	-0.007	0.010[a] 0.002[b] -0.009[c] -0.014[d]

	nbu	0.001	0.047	0.002	0.013 [a] 0.006 [b] -0.004 [c] -0.008[d]	-0.015	0.047	-0.008	0.009 [a] 0.001 [b] -0.010 [c] -0.014 [d]
D2A2	*me/nhex*	-0.003	0.039	0.004	0.016 [a] 0.012 [b] 0.007 [c] 0.005[d]	-0.024	0.032	-0.018	0.003 [a] -0.002 [b] -0.008 [c] -0.010 [d]
D2A3	*nbu*	0.014	0.030	-0.008	0.014[a] 0.011[b] 0.007[c] 0.006[d]	-0.004	0.019	-0.034	-0.001 [a] -0.004 [b] -0.008 [c] -0.010 [d]
	nbu(O)	0.005	0.033	-0.014	0.012 [a] 0.009 [b] 0.004 [c] 0.003[d]	-0.020	0.021	-0.045	-0.005 [a] -0.009 [b] -0.015 [c] -0.016 [d]
	nbu(S)	0.002	0.030	-0.018	0.010 [a] 0.007 [b] 0.002 [c] 0.001[d]	-0.025	0.015	-0.051	-0.010 [a] -0.014 [b] -0.019 [c] -0.021 [d]

[e]B2PLYP/def2-TZVP

Table S4: d_{BLA} values of the charged ground state as derived from DFT (ωB97X-D/36-311G**, gas), C-DFT (CAM-B3LYP-D3/6-311G**, $\delta^{D/A}$=±0.6q) and DFT/PCM (ωB97X-D/6-311G**, a = chloroform, b = THF, c = acetone, d = DMSO).

		d_{BLA} average Å			d_{BLA} central Å		
class	side chain	0: DFT gas +1: (U)DFT gas	0: C-DFT gas +1: C-DFT gas	0: DFT PCM +1: (U)DFT PCM	0: DFT gas +1 :(U)DFT gas	0: C-DFT gas +1: C-DFT gas	0: DFT PCM +1: (U)DFT PCM
D1A1	*pyrl*	-0.019	-0.018	-0.015 [a] -0.014 [b] -0.014 [c] -0.013 [d]	-0.028	-0.026	-0.021 [a] -0.019 [b] -0.016 [c] -0.015 [d]
	et/bu	-0.018	-0.017	-0.012 [d]	-0.027	-0.025	-0.015 [d]
	nbu-P1	-0.019	-0.018	-0.012 [d]	-0.028	-0.026	-0.015 [d]
	nbu-P2						
	nbu-P3						
	nhex	-0.018	-0.017	-0.011 [d]	-0.027	-0.025	-0.014 [d]
D1A2	*nhex/mePh*	-0.019	-0.020	-0.013 [d]	0.007	0.004	0.021 [d]
D1A3	*et*	-0.002	-0.003	-0.003 [d]	0.038	0.036	0.043 [d]
D2A1	*nhex*	-0.017	-0.027	-0.019 [d]	-0.052	-0.056	-0.063 [d]
	nbu	-0.030	-0.027	-0.020 [d]	-0.059	-0.057	-0.064 [d]
D2A2	*me/nhex*	-0.015	-0.014	-0.009 [a] -0.008 [b] -0.007 [c] -0.006 [d]	-0.040	-0.038	-0.036 [a] -0.035 [b] -0.034 [c] -0.033 [d]
D2A3	*nbu*	0.011	0.012	0.013 [a] 0.013 [b] 0.013 [c] 0.013 [d]	-0.012	-0.010	-0.009 [a] -0.009 [b] -0.009 [c] -0.009 [d]
	nbu(O)	0.001	0.002	0.004 [d]	-0.028	-0.026	-0.024 [d]
	nbu(S)	0.005	0.006	0.008 [d]	-0.025	-0.023	-0.022 [d]

Table S5: d_{BLA} values of the neutral and charged ground state as derived from C-DFT (CAM-B3LYP-D3/6-311G**, $\delta^{D/A}$=±0.6q) and DFT/PCM (ωB97X-D/6-311G**/DMSO).

		$d_{BLA}^{average}$	$d_{BLA}^{average}$ neutral GS Å		$d_{BLA}^{average}$ charged GS Å	
class	side chain	X-Ray	C-DFT gas	DFT DMSO	C-DFT gas	DFT DMSO
D1A1	*pyrl*	-0.009	-0.010	-0.015	-0.018	-0.013
	et/bu	-0.012	-0.010	-0.013	-0.017	-0.012
	nbu-P1	-0.003	-0.010	-0.013	-0.018	-0.012
	nbu-P2	-0.010				
	nbu-P3	-0.023				
	nhex	-0.017	-0.010	-0.013	-0.017	-0.011
D1A2	*nhex/mePh*	-0.016	-0.025	-0.018	-0.020	-0.013
D1A3	*et*	-0.017	-0.028	-0.011	-0.003	-0.003
D2A1	*nhex*	-0.002	0.003	-0.007	-0.027	-0.019
	nbu	0.001	0.002	-0.008	-0.027	-0.020
D2A2	*me/nhex*	-0.003	0.004	0.005	-0.014	-0.006
D2A3	*nbu*	0.014	-0.008	0.006	0.012	0.013
	nbu(O)	0.005	-0.014	0.003	0.002	0.004
	nbu(S)	0.002	-0.018	0.001	0.006	0.008

2. Crystal Supercell Analysis

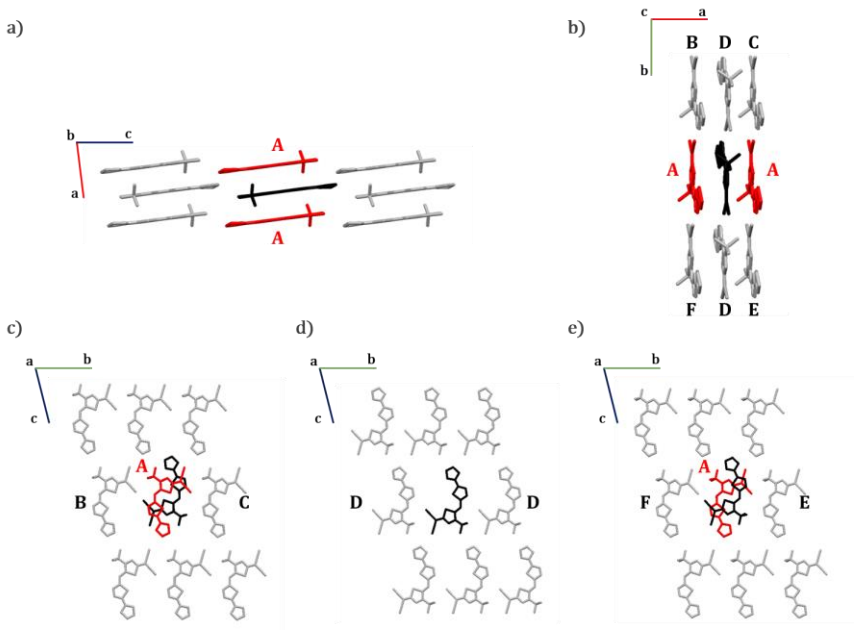

Figure S4: Different views of a supercell of the crystal structure of *pyrl*-**D1A1**. The central molecule (black) and nearest neighbours (red) showing large V_{ij} (i.e., V_{ij} >10 meV). Further nearest neighbors considered in the kinetic Monte Carlo simulations are labelled B – F.

Table S6: Computed (ωB97X-D3/6-311G**) charge transfer integrals (V_{ij}), distances between the centre of mass (CoM) and Brownian transfer rates (k_{eT}) as calculated with the Marcus and Marcus-Levich-Jortner (MLJ) theory for each dimer belonging to *pyrl*-**D1A1**.

dimer	$\|V_{ij}\|$ (meV)	CoM (Å)	k_{eT} (s^{-1}) Marcus	k_{eT} (s^{-1}) MLJ
A	56	3.64	2.2×10^{13}	4.7×10^{13}
B	2	9.15	3.3×10^{10}	6.9×10^{10}
C	2	9.25	3.0×10^{10}	6.3×10^{10}
D	2	9.87	2.8×10^{10}	5.8×10^{10}
E	4	11.66	9.3×10^{10}	1.9×10^{11}
F	3	11.73	7.4×10^{10}	1.5×10^{11}

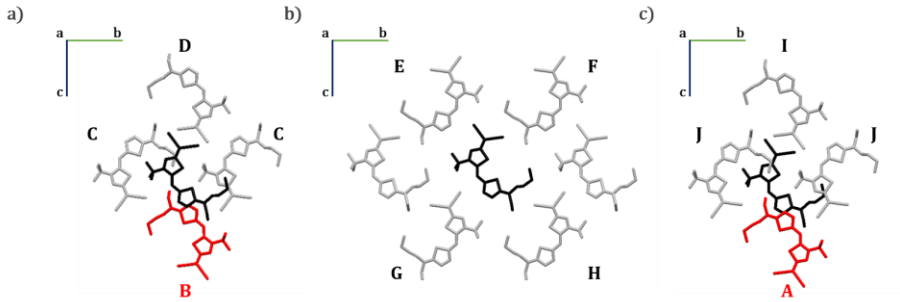

Figure S5: Different views of a supercell of the crystal structure of *etbu*-**D1A1**. The central molecule (black) and nearest neighbours (red) showing large V_{ij} (i.e., V_{ij} >10 meV). Further nearest neighbors considered in the kinetic Monte Carlo simulations are labelled C – J.

Table S7: Computed (ωB97X-D3/6-311G**) charge transfer integrals (V_{ij}), distances between the centre of mass (CoM) and Brownian transfer rates (k_{eT}) as calculated with the Marcus and Marcus-Levich-Jortner (MLJ) theory for each dimer belonging to *etbu*-**D1A1**.

dimer	$\|V_{ij}\|$ (meV)	CoM (Å)	k_{eT} (s^{-1}) Marcus	k_{eT} (s^{-1}) MLJ
A	14	8.43	1.3×10^{12}	9.6×10^{11}
B	18	8.70	2.0×10^{12}	1.5×10^{12}
C	2	8.38	2.2×10^{10}	1.7×10^{10}
D	4	11.72	8.1×10^{10}	6.2×10^{10}
E	6	11.41	2.4×10^{11}	1.9×10^{11}
F	3	12.41	6.6×10^{10}	5.0×10^{10}
G	5	11.42	1.4×10^{11}	1.1×10^{11}
H	8	14.41	3.6×10^{11}	2.8×10^{11}
I	5	12.11	1.3×10^{11}	9.9×10^{10}
J	3	8.412	6.1×10^{10}	4.6×10^{10}

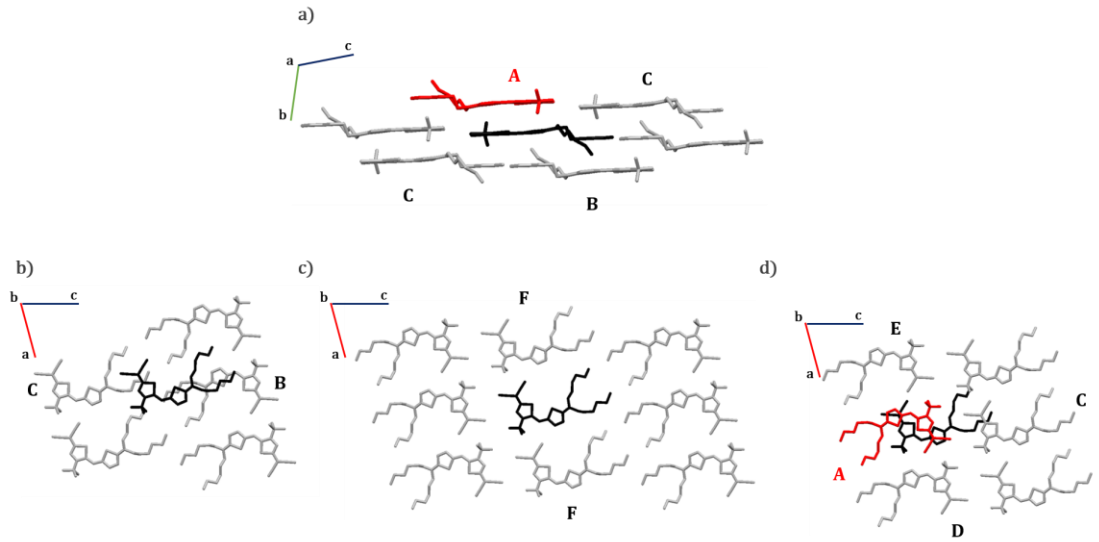

Figure S6: Different views of a supercell of the crystal structure of *nhex*-**D1A1**. The central molecule (black) and nearest neighbours (red) showing large V_{ij} (i.e., V_{ij} >10 meV). Further nearest neighbors considered in the kinetic Monte Carlo simulations are labelled B – F.

Table S8: Computed (ωB97X-D3/6-311G**) charge transfer integrals (V_{ij}), distances between the centre of mass (CoM) and Brownian transfer rates (k_{eT}) as calculated with the Marcus and Marcus-Levich-Jortner (MLJ) theory for each dimer belonging to *nhex*-**D1A1**.

dimer	$\|V_{ij}\|$ (meV)	CoM (Å)	k_{eT} (s^{-1}) Marcus	k_{eT} (s^{-1}) MLJ
A	23	6.35	3.9×10^{12}	9.1×10^{12}
B	3	8.26	6.7×10^{10}	1.6×10^{11}
C	8	13.41	5.1×10^{11}	1.2×10^{12}
D	4	10.74	9.4×10^{10}	2.2×10^{11}
E	6	12.52	2.4×10^{11}	5.6×10^{11}
F	3	9.78	6.3×10^{10}	1.5×10^{11}

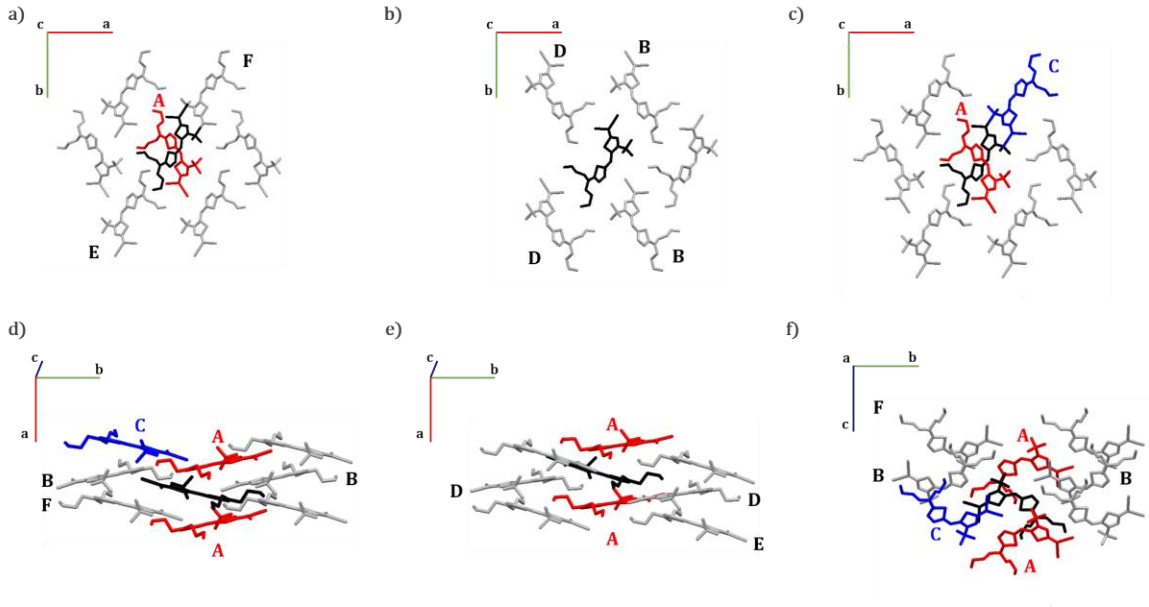

Figure S7: Different views of a supercell of the crystal structure of *nbu-P1*-**D1A1**. The central molecule (black) and nearest neighbours (red and blue) showing large V_{ij} (i.e., V_{ij} >10 meV). Further nearest neighbors considered in the kinetic Monte Carlo simulations are labelled D – F.

Table 9: Computed (ωB97X-D3/6-311G**) charge transfer integrals (V_{ij}), distances between the centre of mass (CoM) and Brownian transfer rates (k_{eT}) as calculated with the Marcus and Marcus-Levich-Jortner (MLJ) theory for each dimer belonging to *nbu-P1*-**D1A1**.

dimer	$\|V_{ij}\|$ (meV)	CoM (Å)	k_{eT} (s^{-1}) Marcus	k_{eT} (s^{-1}) MLJ
A	14	5.09	1.5×10^{12}	2.3×10^{12}
B	2	11.85	2.7×10^{10}	4.2×10^{10}
C	10	10.44	6.6×10^{11}	1.0×10^{12}
D	1	12.42	1.1×10^{10}	1.8×10^{10}
E	3	12.90	8.0×10^{10}	1.3×10^{11}
F	2	13.19	4.0×10^{10}	6.2×10^{10}

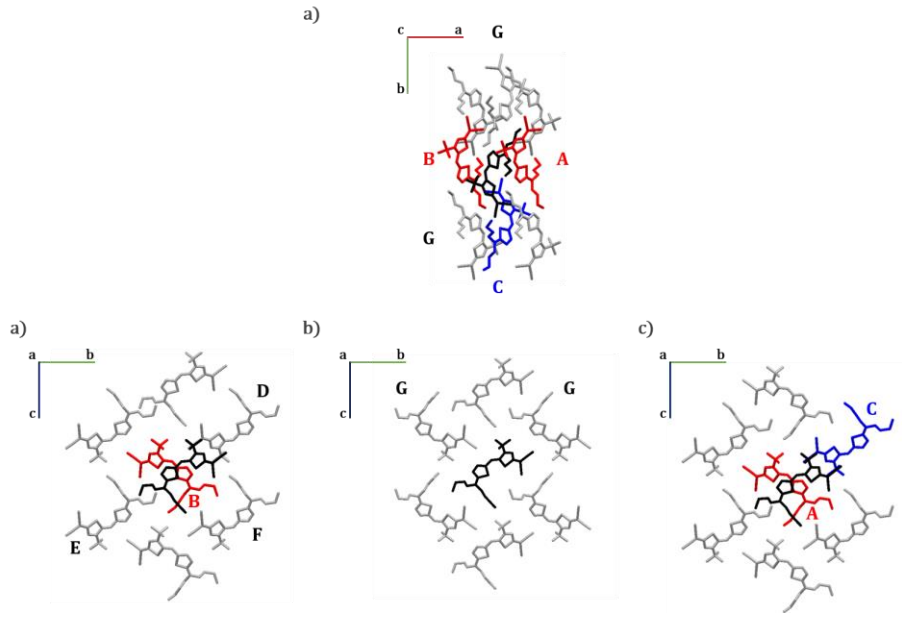

Figure S8: Different views of a supercell of the crystal structure of *nbu-P2*-**D1A1**. The central molecule (black) and nearest neighbours (red) showing large V_{ij} (i.e., V_{ij} >10 meV). Further nearest neighbors considered in the kinetic Monte Carlo simulations are labelled D – G.

Table S10: Computed (ωB97X-D3/6-311G**) charge transfer integrals (V_{ij}), distances between the centre of mass (CoM) and Brownian transfer rates (k_{eT}) as calculated with the Marcus and Marcus-Levich-Jortner (MLJ) theory for each dimer belonging to *nbu-P2*-**D1A1**.

dimer	$\|V_{ij}\|$ (meV)	CoM (Å)	k_{eT} (s^{-1}) Marcus	k_{eT} (s^{-1}) MLJ
A	20	4.95	3.0×10^{12}	4.4×10^{12}
B	15	5.05	1.7×10^{12}	2.6×10^{12}
C	50	10.27	1.9×10^{13}	2.7×10^{13}
D	4	11.70	1.0×10^{11}	1.5×10^{11}
E	3	13.41	6.8×10^{10}	1.0×10^{11}
F	5	10.03	1.5×10^{11}	2.2×10^{11}
G	5	11.67	2.1×10^{11}	3.2×10^{11}

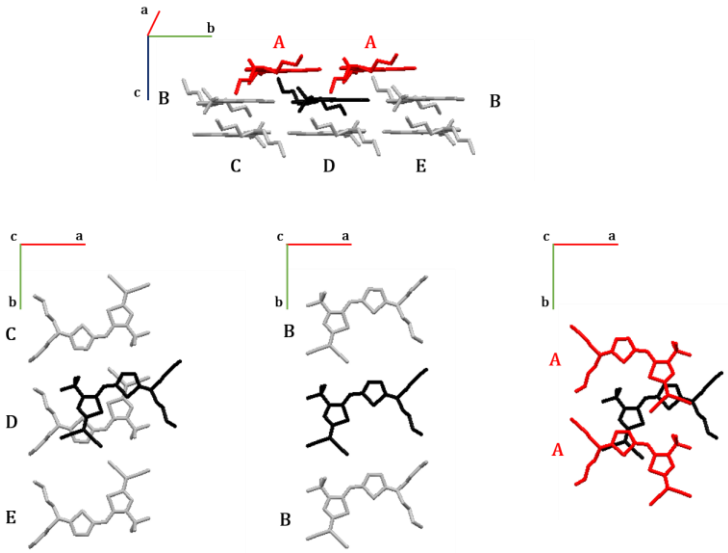

Figure S9: Different views of a supercell of the crystal structure of *nbu-P3*-**D1A1**. The central molecule (black) and nearest neighbours (red) showing large V_{ij} (i.e., V_{ij} >10 meV). Further nearest neighbors considered in the kinetic Monte Carlo simulations are labelled B – E.

Table S11: Computed (ωB97X-D3/6-311G**) charge transfer integrals (V_{ij}), distances between the centre of mass (CoM) and Brownian transfer rates (k_{eT}) as calculated with the Marcus and Marcus-Levich-Jortner (MLJ) theory for each dimer belonging to *nbu-P3*-**D1A1**.

dimer	$\|V_{ij}\|$ (meV)	CoM (Å)	k_{eT} (s^{-1}) Marcus	k_{eT} (s^{-1}) MLJ
A	35	6.60	9.0×10^{12}	1.5×10^{12}
B	6	10.07	2.8×10^{11}	4.5×10^{11}
C	7	12.66	3.4×10^{11}	5.4×10^{11}
D	8	4.80	4.7×10^{11}	7.5×10^{11}
E	5	9.40	2.0×10^{11}	3.2×10^{11}

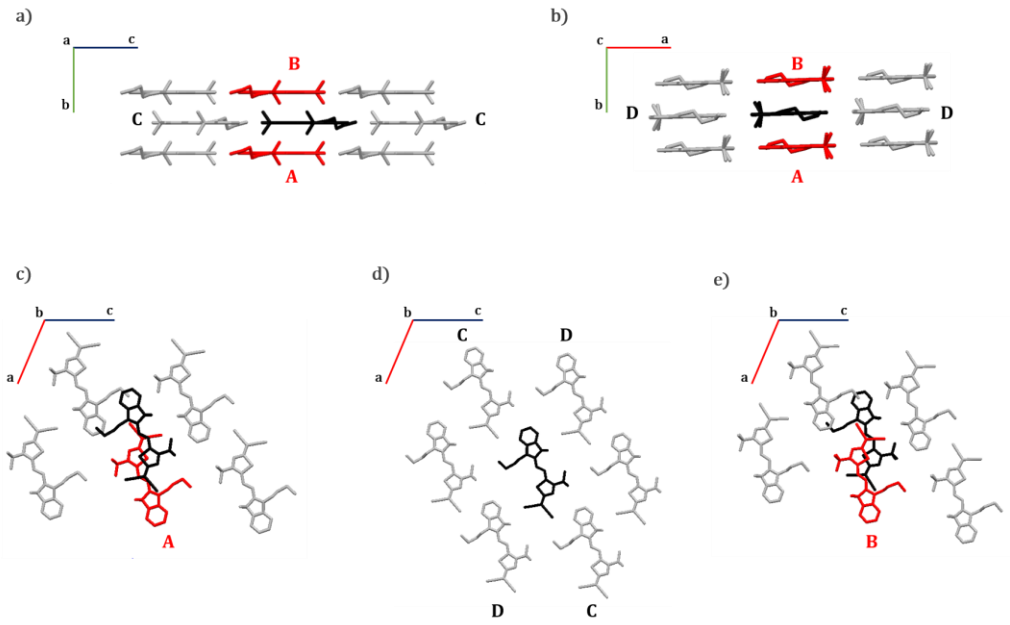

Figure S10: Different views of a supercell of the crystal structure of *nbu-P2*-**D2A1**. The central molecule (black) and nearest neighbours (red) showing large V_{ij} (i.e., V_{ij} >10 meV). Further nearest neighbors considered in the kinetic Monte Carlo simulations are labelled C – D.

Table S12: Computed (ωB97X-D3/6-311G**) charge transfer integrals (V_{ij}), distances between the centre of mass (CoM) and Brownian transfer rates (k_{eT}) as calculated with the Marcus and Marcus-Levich-Jortner (MLJ) theory for each dimer belonging to *nbu*-**D2A1**.

dimer	$\|V_{ij}\|$ (meV)	CoM (Å)	k_{eT} (s^{-1}) Marcus	k_{eT} (s^{-1}) MLJ
A	16	6.26	1.0×10^{12}	1.0×10^{12}
B	11	6.26	4.9×10^{11}	2.2×10^{11}
C	3	14.78	3.6×10^{10}	7.5×10^{10}
D	4	12.63	7.3×10^{10}	1.6×10^{11}

3. Crystallographic Data

Table S13: Crystallographic Parameters of the different unit cells of *nbu-Pn*-**D1A1**.

	nbu-Pn-**D1A1**		
	P1	*P2*	*P3*
Temp. (K)	300	100	100
CCDC	2073437	2073438	2073461
a (Å)	13.09	13.94	38.07
b (Å)	19.30	18.85	10.07
c (Å)	9.84	9.08	13.71
α (°)	90.00	90.00	90.00
β (°)	101.70	105.60	102.30
γ (°)	90.00	90.00	90.00
Z	4	4	8
Space Group	$P2_1/c$	$P2_1/c$	C2/c

4. Huang Rhys Factor Analysis

Table S14: Huang Rhys factor analysis of **D1A1** and **D2A1** based on the geometries obtained by C-DFT (CAM-B3LYP-D3/6-311G**, $\delta^{D/A}$=±0.6q) calculations.

class	side chain	λ_i^{AP} meV	cutoff cm^{-1}	λ_i^{HR} meV	S_{eff}	ω_{eff} cm^{-1}
D1A1	*pyrl*	127	0	127	1.449	901
	et/bu	140	0	168	3.2528	416
			200	161	1.2359	1053
	nbu-P1	126	0	125	1.4582	692
	nbu-P2	126	0	125	1.5356	656
	nbu-P3	125	0	125	1.4157	715
	nhex	123	0	123	0.9503	1043
D2A1	*nbu*	177	0	176	1.7541	807

5. Validity of non-adiabatic transfer model

The validity of the non-adiabatic transfer model was verified by computing the adiabaticity factor ξ, defined as $\xi = 2V_{ij}/\lambda^{tot}$. For the majority of the merocyanines here investigated, ξ lies between 0.01 and 0.2, thus supporting a non-adiabatic (or small polaron hopping) transport regime.[S5] Only for the case of *pyrl*-**D1A1** we obtained ξ = 0.63 considering the highest V_{ij} = 56 meV and a λ^{tot} ~177 meV. This value may possibly lead to a deviation from the small polaron model, however, as well documented in literature for similar cases, the non-adiabatic scheme can still be reasonably applied resulting in charge mobility values approaching the experimental data.

6. Preliminary evaluation of the impact of thermal effects onto the electronic couplings

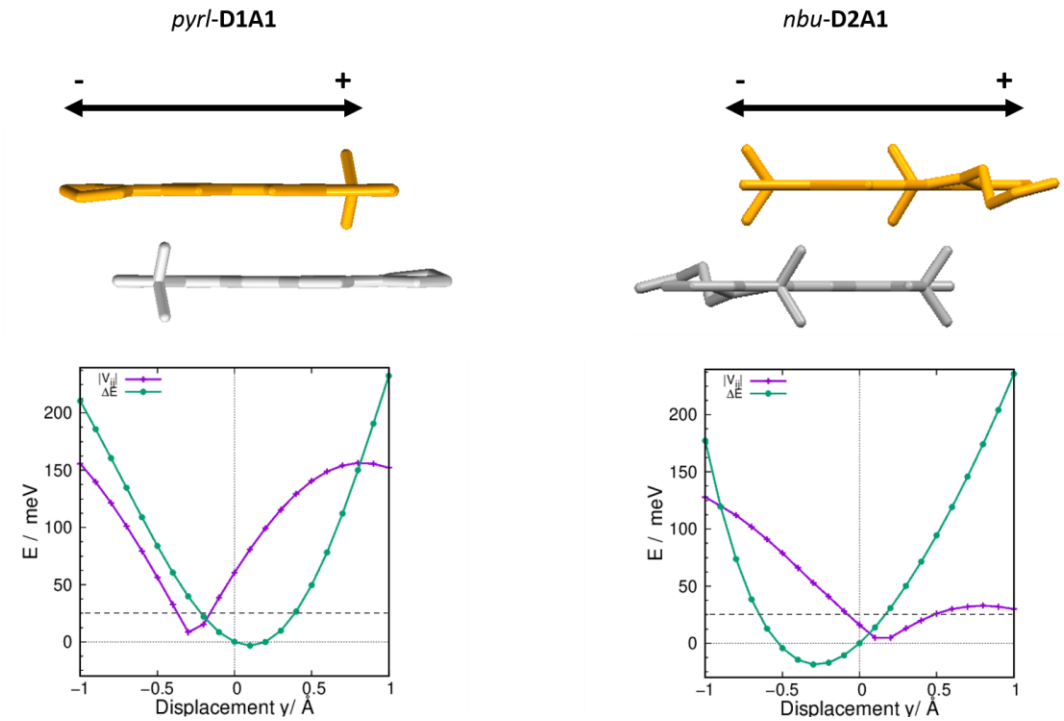

Figure S11: Dimers showing the highest coupling for *pyrl*-**D1A1** (left) and *nbu*-**D2A1** (right). The orange molecule was translated along the long axes in steps of 0.1 Å. Computed absolute V_{ij} values (purple) for each translating step, as well as site energy differences (ΔE) (green), as compared to the crystal equilibrium

position at 0 Å. Dotted horizontal grey line sets the value for the thermal energy (k_BT = 25 meV).

7. Charge mobilities as calculated by the Marcus approach

Table S15: Computed charge mobilities evaluated by assuming a Brownian diffusion mechanisms *via* the Einstein-Smoluchowski equation (μ^0), and an application of an electric field ($\mu(E)$, E = 10^5 V cm^{-1}). Reported is the Marcus approach.

class	side chain	μ^0 ($cm^2V^{-1}s^{-1}$) Marcus	$\mu(E)^b$ ($cm^2V^{-1}s^{-1}$) Marcus
D1A1	*pyrl*	0.343	0.978
	et/bu	0.167	0.296
	nbu-P1	0.104	0.147
	nbu-P2	0.355	0.755
	nbu-P3	0.379	1.097
	nhex	0.153	0.343
D2A1	*nbu*	0.041	0.056

8. Directionality of the computed charge mobilities (kMC trajectories).

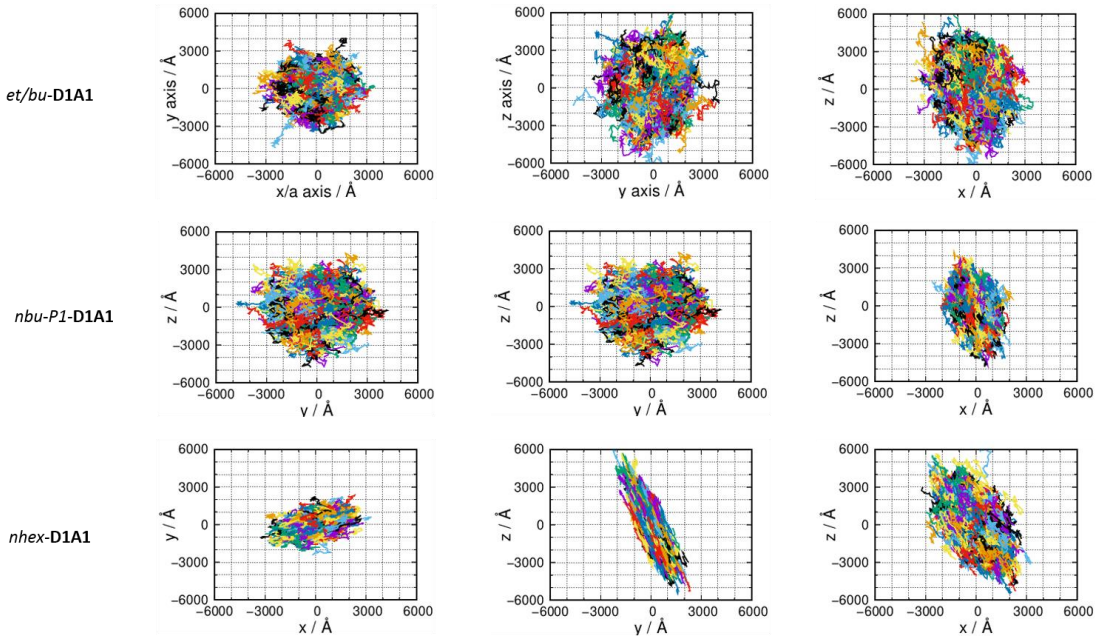

Figure S12: Plot of 1000 kMC trajectories (each consisting of 10^5 steps) for **D1A1** class (from top to bottom: *et/bu*-, *nbu-P1* and *nhex*-**D1A1**). Trajectories are reported for the three Cartesian planes, namely *yx*, *zy* and *zx*.

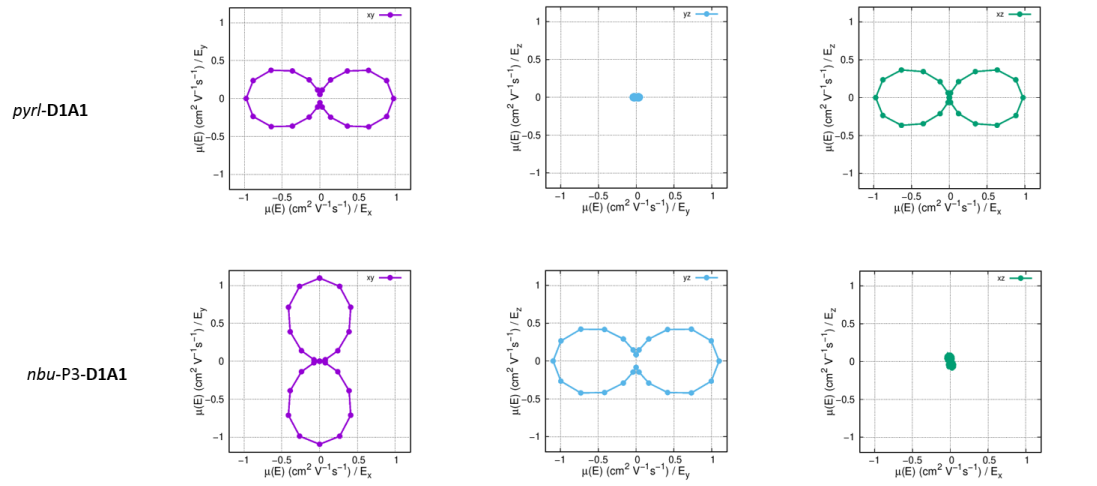

Figure S13: Charge mobility μ(*E*) (*E* = 10^5 V cm^{-1}) within the Marcus theory along the electric field vector, which is rotated within the *xy*, *xz* and *yz* plane in steps of 15°. Top: *pyrl*-**D1A1** Bottom: *nbu-P3*-**D1A1**.

Table S16: Computed charge mobilities (hole, μ) of **D1A1** and **D2A1** evaluated by assuming a Brownian diffusion mechanisms (μ^0) and an application of an electric field ($\mu(E)$ E = 10^5 V cm^{-1}). The charge mobility is reported for the 3 cartesian directions x, y and z, as well as the average mobility overall and for $\mu(E)$ simulations the average of the different planes is reported as well.

	direction	**D1A1**						**D2A1**
		pyrl	*et/bu*	*nbu-P1*	*nbu-P2*	*nbu-P3*	*nhex*	*nbu*
μ^0 ($cm^2V^{-1}s^{-1}$) Marcus	**x**	0.975	0.106	0.034	0.221	0.004	0.102	0.055
	y	0.054	0.109	0.134	0.761	1.051	0.046	0.037
	z	0.000	0.287	0.143	0.083	0.083	0.311	0.032
	average_xyz	0.343	0.167	0.104	0.355	0.379	0.153	0.041
μ^0 ($cm^2V^{-1}s^{-1}$) MLJ	x	2.041	0.083	0.055	0.312	0.006	0.248	0.121
	y	0.113	0.083	0.205	1.078	1.727	0.106	0.077
	z	0.000	0.228	0.226	0.128	0.136	0.743	0.075
	average_xyz	0.718	0.131	0.162	0.506	0.623	0.366	0.091
$\mu(E)$ ($cm^2V^{-1}s^{-1}$) Marcus	x[a]	0.978	0.103	0.034	0.213	0.004	0.105	0.056
	y[b]	0.054	0.109	0.136	0.756	1.097	0.046	0.036
	z[c]	0.004	0.296	0.142	0.086	0.084	0.317	0.035
	average_xy[d]	0.516	0.106	0.085	0.485	0.551	0.075	0.046
	average_xz[e]	0.491	0.199	0.088	0.149	0.044	0.211	0.045
	average_yz[f]	0.029	0.202	0.139	0.421	0.591	0.181	0.035
	average_xyz[g]	0.345	0.169	0.104	0.352	0.395	0.156	0.042
$\mu(E)$ ($cm^2V^{-1}s^{-1}$) MLJ	x[a]	2.075	0.079	0.060	0.356	0.007	0.247	0.125
	y[b]	0.113	0.083	0.235	1.263	1.936	0.109	0.082
	z[c]	0.009	0.226	0.245	0.143	0.149	0.743	0.075
	average_xy[d]	1.094	0.081	0.147	0.810	0.971	0.178	0.103
	average_xz[e]	1.042	0.152	0.153	0.250	0.078	0.495	0.100
	average_yz[f]	0.061	0.155	0.240	0.703	1.042	0.426	0.078
	average_xyz[g]	0.732	0.129	0.180	0.588	0.697	0.366	0.094

[a]$\mu(E)$ for the electric field vector along (100)[a], (010)[b] and (001)[c]. Averaged $\mu(E)$ for the electric field vector along (100) and (010)[d], (100) and (001)[e], (010) and (001)[f], (100), (010) and (001)[g].

9. Parameter variation in charge mobility simulations.

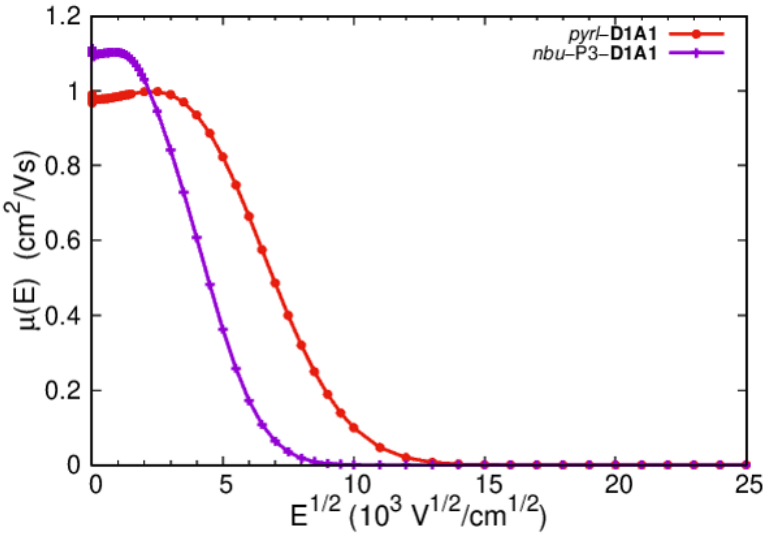

Figure S14: Dependency of μ(*E*) (as computed at the Marcus level) by varying the electric field *E*, for *pyrl*-**D1A1** and *nbu-P3*-**D1A1**.

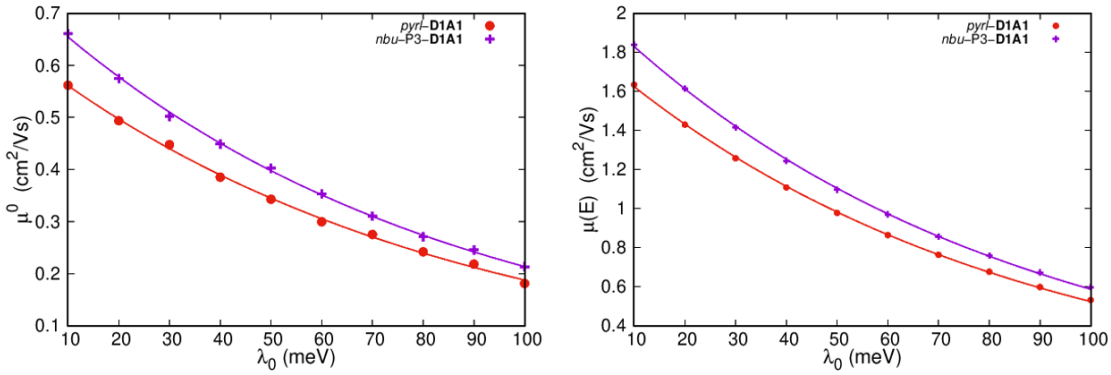

Figure S15: Dependency of the zero field mobility μ^0 (left) and μ(*E*) (right, $E = 10^5$ V cm^{-1}) (as computed at the Marcus level) with respect to the variation of the outer reorganization energy λ_0, for *pyrl*-**D1A1** and *nbu*-P3-**D1A1**.

10.Evaluation of *nbu-P4*-D1A1

Table S17: Computed (ωB97X-D3/6-311G**) charge transfer integral (V_{ij}), distance between the centre of mass (CoM) and Brownian transfer rate (k_{eT}) as calculated with the Marcus-Levich-Jortner (MLJ) theory for polymorph *nbu-P4*-**DA1**.

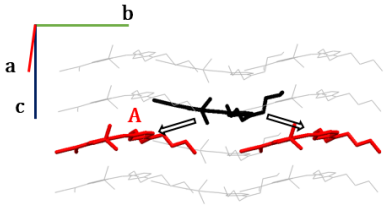

dimer	$\|V_{ij}\|$ (meV)	CoM (Å)	k_{eT} (s^{-1}) MLJ	μ^0 ($cm^2V^{-1}s^{-1}$) MLJ
A	36	10.23	1.7×10^{13}	1.728

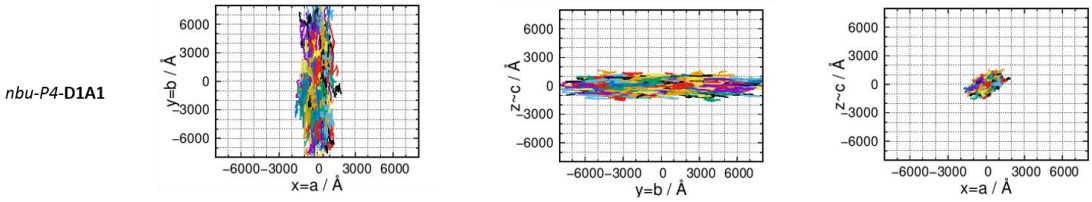

Figure S16: Plot of 1000 kMC trajectories (each consisting of 10^5 steps) for *nbu-P4*-**D1A1**. Trajectories are reported for the three Cartesian planes, namely *yx*, *zy* and *zx*.

11. Experimental Details

Sample fabrication. *nbu*-**D1A1** was dissolved in chloroform (*Fisher Chemicals*, HPLC grade) with a concentration of C = $1 \cdot 10^{-2}$ mol/l. A volume of 0.1 ml of the solution was spin coated on commercially available OFET substrates (*Fraunhofer IPMS*), which were ozonized for ten minutes before use, to enhance the surface polarity and thus improve *nbu*-**D1A1** film coverage. The spin coating process was performed under static dispense with 3000 rpm speed, 3000 rpm/s acceleration, and 60 seconds spinning time. With these parameters film thicknesses of approximately 20 nm were obtained. The subsequent annealing was performed by placing the substrates on a preheated hot-plate directly after the spin coating process and removing them after 10 minutes. The set temperatures are mentioned in the main text.

Electrical characterization. Transistor measurements were conducted with a *Keithley, 4200A-SCS Parameter Analyzer*. In this study, for every sample usually four, but if a device showed shortcuts, at least three devices with a channel-length of 20 µm were used for evaluation. The charge carrier mobility was determined from transfer characteristics in the linear regime using the formula $\mu_{linear} = \frac{\partial I_D}{\partial V_G}\frac{L}{WC_{SiO_2}V_D}$, where μ_{linear} is the hole mobility in the linear regime, I_D is the drain-current, V_G is the gate-voltage, L and W are the channel-length and –width, C_{SiO_2} is the gate-dielectric capacitance per unit area, and V_D is the drain-voltage. The derivative was evaluated by linear fitting of plots of the drain-current in dependence on the gate-voltage in the linear regime (fitting range: V_G: (−20 V) – (−50 V)). The corresponding transfer characteristics were recorded from +10 V to -50 V gate-voltage, at a constant drain voltage of -10 V.

12. Computational Methods

All DFT calculations were performed within the Gaussian16 program version C.01.[S3] The constrained DFT (C-DFT) calculations were performed with NWChem version 6.8,[S4] using the CAM-B3LYP functional with D3 dispersion and the 6-311G** basis set.

ESI REFERENCES

S1. Rühle, V.; Lukyanov, A.; May, F.; Schrader, M.; Vehoff, T.; Kirkpatrick, J.; Baumeier, B.; Andrienko, D., Microscopic Simulations of Charge Transport in Disordered Organic Semiconductors. *Journal of Chemical Theory and Computation* **2011**, *7*, 3335-3345.

S2. Poelking, C.; Cho, E.; Malafeev, A.; Ivanov, V.; Kremer, K.; Risko, C.; Brédas, J.-L.; Andrienko, D., Characterization of Charge-Carrier Transport in Semicrystalline Polymers: Electronic Couplings, Site Energies, and Charge-Carrier Dynamics in Poly(Bithiophene-Alt-Thienothiophene) [Pbttt]. *The Journal of Physical Chemistry C* **2013**, *117*, 1633-1640.

S3 Gaussian 16, Revision C.01, M. J. Frisch, G. W. Trucks, H. B. Schlegel, G. E. Scuseria, M. A. Robb, J. R. Cheeseman, G. Scalmani, V. Barone, G. A. Petersson, H. Nakatsuji, X. Li, M. Caricato, A. V. Marenich, J. Bloino, B. G. Janesko, R. Gomperts, B. Mennucci, H. P. Hratchian, J. V. Ortiz, A. F. Izmaylov, J. L. Sonnenberg, D. Williams-Young, F. Ding, F. Lipparini, F. Egidi, J. Goings, B. Peng, A. Petrone, T. Henderson, D. Ranasinghe, V. G. Zakrzewski, J. Gao, N. Rega, G. Zheng, W. Liang, M. Hada, M. Ehara, K. Toyota, R. Fukuda, J. Hasegawa, M. Ishida, T. Nakajima, Y. Honda, O. Kitao, H. Nakai, T. Vreven, K. Throssell, J. A. Montgomery, Jr., J. E. Peralta, F. Ogliaro, M. J. Bearpark, J. J. Heyd, E. N. Brothers, K. N. Kudin, V. N. Staroverov, T. A. Keith, R. Kobayashi, J. Normand, K. Raghavachari, A. P. Rendell, J. C. Burant, S. S. Iyengar, J. Tomasi, M. Cossi, J. M. Millam, M. Klene, C. Adamo, R. Cammi, J. W. Ochterski, R. L. Martin, K. Morokuma, O. Farkas, J. B. Foresman, and D. J. Fox, Gaussian, Inc., Wallingford CT, 2016.

S4 E. Aprà, E. J. Bylaska, W. A. de Jong, N. Govind, K. Kowalski, T. P. Straatsma, M. Valiev, H. J. J. van Dam, Y. Alexeev, J. Anchell, V. Anisimov, F. W. Aquino, R. Atta-Fynn, J. Autschbach, N. P. Bauman, J. C. Becca, D. E. Bernholdt, K. Bhaskaran-Nair, S. Bogatko, P. Borowski, J. Boschen, J. Brabec, A. Bruner, E. Cauët, Y. Chen, G. N. Chuev, C. J. Cramer, J. Daily, M. J. O. Deegan, T. H. Dunning Jr., M. Dupuis, K. G. Dyall, G. I. Fann, S. A. Fischer, A. Fonari, H. Früchtl, L. Gagliardi, J. Garza, N. Gawande, S. Ghosh, K. Glaesemann, A. W. Götz, J. Hammond, V. Helms, E. D. Hermes, K. Hirao, S. Hirata, M. Jacquelin, L. Jensen, B. G. Johnson, H. Jónsson, R. A. Kendall, M. Klemm, R. Kobayashi, V. Konkov, S. Krishnamoorthy, M. Krishnan, Z.

Lin, R. D. Lins, R. J. Littlefield, A. J. Logsdail, K. Lopata, W. Ma, A. V. Marenich, J. Martin del Campo, D. Mejia-Rodriguez, J. E. Moore, J. M. Mullin, T. Nakajima, D. R. Nascimento, J. A. Nichols, P. J. Nichols, J. Nieplocha, A. Otero-de-la-Roza, B. Palmer, A. Panyala, T. Pirojsirikul, B. Peng, R. Peverati, J. Pittner, L. Pollack, R. M. Richard, P. Sadayappan, G. C. Schatz, W. A. Shelton, D. W. Silverstein, D. M. A. Smith, T. A. Soares, D. Song, M. Swart, H. L. Taylor, G. S. Thomas, V. Tipparaju, D. G. Truhlar, K. Tsemekhman, T. Van Voorhis, Á. Vázquez-Mayagoitia, P. Verma, O. Villa, A. Vishnu, K. D. Vogiatzis, D. Wang, J. H. Weare, M. J. Williamson, T. L. Windus, K. Woliński, A. T. Wong, Q. Wu, C. Yang, Q. Yu, M. Zacharias, Z. Zhang, Y. Zhao, and R. J. Harrison, "NWChem: Past, present, and future", *The Journal of Chemical Physics* **152**, 184102 (2020). DOI: 10.1063/5.0004997

S5. Oberhofer, H.; Reuter, K.; Blumberger, J., Charge Transport in Molecular Materials: An Assessment of Computational Methods. *Chemical Reviews* **2017**, *117*, 10319-10357.